AIMS Materials Science, 11(4): 802–814.
DOI: 10.3934/matersci.2024039
Received: 25 July 2024
Revised: 08 September 2024
Accepted: 11 September 2024
Published: 13 September 2024

https://www.aimspress.com/journal/Materials

Research article

Enhancement of ferroelectricity in perovskite $BaTiO_3$ epitaxial thin films by sulfurization

Xuan Luc Le, Nguyen Dang Phu and Nguyen Xuan Duong*

Faculty of Electronics and Telecommunications, VNU University of Engineering and Technology, E3 Building, 144 Xuan Thuy, Hanoi 100000, Vietnam

* **Correspondence:** Email: nxduong@vnu.edu.vn.

Abstract: Sulfur is a promising anion dopant for exploring exotic physical phenomena in complex perovskite oxides. However, sulfurization to the epitaxial single-crystal oxide thin films with high crystallinity is experimentally challenging due to the volatility of sulfur element; thus, sulfurization effects on the associated properties have been scarcely studied. Here, we demonstrate an enhancement of ferroelectric polarization of epitaxial $BaTiO_3$ thin films by sulfur doping. Initially, the epitaxial $BaTiO_3$ thin films with high crystallinity were grown by pulsed laser deposition (PLD). Then, sulfurization to epitaxial $BaTiO_3$ films was performed using a precursor of thiourea (CH_4N_2S) solution via a spin-coating technique. The crystalline structure of sulfurized $BaTiO_3$ films was identified by X-ray diffraction (XRD) and scanning transmission electron microscopy (STEM). The structural distortion with the elongated out-of-plane lattice constant was observed in the sulfurized $BaTiO_3$ films. Atomic force microscopy (AFM) analyses also confirmed the surface morphology of films after sulfurization. Interestingly, we found an enhanced ferroelectric polarization in sulfur-doped $BaTiO_3$ films accompanying the improved tetragonality in the crystal structure after sulfurization. The increments in the remnant (~34.8%) and saturated (~30.6%) polarizations of sulfurized $BaTiO_3$ films were obtained in comparison with pure $BaTiO_3$ films. Our work could be a primary study for a thorough understanding of the sulfur doping effect in perovskite oxides, opening up the potential of oxysulfide materials.

Keywords: sulfurization; perovskite oxides; ferroelectricity; epitaxy; thin film

1. Introduction

Exploring fascinating physical properties in perovskite oxides (ABO_3, where A- and B-sites are cations) is of great interest for the realization of novel multifunctional devices [1–3]. Among the various approaches, chemical doping (i.e., cations and/or oxygen sites in a perovskite system are partially substituted by atoms of other elements) is an effective pathway to achieve exotic phenomena. For the last few decades, a large variety of attractive physical phenomena have been reported in perovskite oxides by chemical substitution such as structural phase transition [4], improved ferroelectricity [5], multiferroic property [6], and metal-insulator transition [7]. Note that most previous theoretical and experimental works have been mainly focused on the modification of related properties by the substitution of cation sites (i.e., A- and B-sites) [3–6]. Meanwhile, up to our knowledge, the effect of chemical doping on the oxygen site of perovskite structure has not been extensively studied.

Sulfur is a promising dopant at the oxygen site of perovskite structures leading to the emergence of intriguing physical properties in complex oxides. Considering the fact that sulfur S ([Ne]$3s^2 3p^4$) and oxygen O ([He]$2s^2 2p^4$) elements are chalcogens with similar chemical characteristics of the outermost electron shells, an oxygen atom can be easily replaced by a sulfur atom [8]. We note that the radius of an oxygen atom (~1.4 Å) is smaller than that of a sulfur atom (~1.8 Å) [9]. When a sulfur atom occupies the oxygen site, the original perovskite unit cell becomes distorted, resulting in the modification in physical properties. Very recently, it has been theoretically demonstrated that perovskite oxysulfide ($ABO_{3-x}S_x$) systems exhibit various attractive properties [8]. With the structural distortion in ferroelectric perovskites by sulfur doping, the enhanced ferroelectricity is predicted with an increase in tetragonality. Furthermore, an optical gap in the electronic band structure can be reduced, indicative of band-gap tuning by sulfurization [8]. Despite theoretical expectations of novel properties by sulfur doping, detailed experimental studies on the sulfurization of perovskite oxides have been rare [10–12]. A systematic investigation is essential to understand the sulfur-doping effect on the associated physical properties of perovskite oxides.

Synthesis of sulfurized perovskite oxides with high crystallinity is highly required to figure out the effect of sulfurization on associated physical properties. Some efforts have been made to investigate the perovskite oxysulfides with bulk and thin-film geometry [10–13]. Up to now, most of the works have been implemented in polycrystalline ceramics and thin films incorporating disorders such as grain boundaries and misfit dislocations [10–12]. We note that it is difficult to clarify the microscopic mechanism of a change in physical properties driven by sulfur doping in the systems with polycrystallinity using experimental analyses. Moreover, a comparison of experimental results obtained in polycrystalline ceramics and thin films with theoretical predictions, which are derived from primitive unit cells by excluding the extrinsic effect of disorders, is unfair and not convincing [8]. However, it is challenging to synthesize single crystals of sulfur-substituted oxides with high crystallinity owing to the evaporation of the sulfur element, which limits the in-depth examination of sulfur doping in complex perovskite oxides [14].

The realization of sulfur-doped perovskite oxides with high crystallinity is a demanding challenge due to the volatility of the sulfur during the fabrication process [14,15]. The earlier reports demonstrate the fabrication of perovskite oxysulfides by the conventional solid-state reaction method. In this method, a high-temperature sintering process (above 1100 °C) is usually performed for the crystallization of samples [10,12,16]. During sintering, a large amount of sulfur atoms is vaporized at such a high

temperature leading to the deficiency of sulfur dopants. In the other experimental approaches, the sulfur doping to complex oxides is carried out via chemical vapor deposition (CVD) and thermal annealing techniques [17–19]. Here, the sulfur atoms from a precursor (e.g., CS_2 and H_2S) are introduced and incorporated into oxide materials through a chemical reaction. Nevertheless, for both methods, the accurate content of sulfur is not controllable during the sulfurization process; thus, the contamination is formed subsequently [17–19]. Due to the limitations of the aforementioned synthesis methods, an alternative experimental strategy should be utilized to implement the sulfurization to high-crystalline perovskite oxides (e.g., an epitaxial single-crystal film) enabling the investigation of the sulfur-doping effect on associated physical properties systematically.

In this work, we experimentally demonstrate the sulfurization of epitaxial $BaTiO_3$ (BTO) perovskite thin films and examine the modification in the ferroelectric property by sulfur doping. The high-crystalline $BaTiO_3$ thin films are sulfurized successfully using a simple spin coating. The incorporated sulfur atoms from a spin-coated thiourea (CH_4N_2S) layer are diffused inside the $BaTiO_3$ films after a thermal treatment. The structural, morphological, and ferroelectric characteristics of sulfur-doped $BaTiO_3$ (BTO-S) thin films are investigated using X-ray diffraction (XRD), scanning transmission electron microscopy (STEM), atomic force microscopy (AFM), and polarization hysteresis analyses. Interestingly, we observed that the ferroelectric polarization is enhanced in $BaTiO_3$ thin films by sulfur doping accompanying an increase of tetragonality in the crystal structure. The observations of enhanced ferroelectricity in the sulfur-doped $BaTiO_3$ films will be discussed in conjunction with a possible origin of microscopic structural distortion induced by sulfurization.

2. Materials and methods

2.1. Growth of epitaxial $BaTiO_3$ thin films

The epitaxial $BaTiO_3/La_{0.7}Sr_{0.3}MnO_3$ heterostructures were grown on the $SrTiO_3$ (STO) (001) substrates using the pulsed laser deposition (PLD) techniques. A pulsed excimer laser (KrF, wavelength of 248 nm) with a fluence of 1.2 J/cm^2 and a repetition rate of 5 Hz was used to generate the plasma plume from ceramic targets. Before the deposition of each layer, the corresponding ceramic target was pre-ablated with a pulsed laser for 5 min. The $La_{0.7}Sr_{0.3}MnO_3$ (LSMO) film was first grown at 670 °C under an oxygen partial pressure of 20 mTorr. Subsequently, the $BaTiO_3$ film was deposited on the LSMO/STO substrate. During the deposition of the pure $BaTiO_3$ film, the substrate temperature and the oxygen partial pressure were maintained at 640 °C and 100 mTorr, respectively. After the deposition, in situ post-annealing was performed at 640 °C for 1 h under ambient oxygen at 100 Torr.

2.2. Preparation of thiourea solution

We synthesized a thiourea solution as a precursor for the sulfurization process, as shown in Figure 1a. The thiourea powder (CH_4N_2S, 99%, Sigma-Aldrich Co.) was mixed with a solvent of distilled water and ethanol. The volume ratio between water and ethanol was 1:4. The mixed solution was stirred for 24 h at room temperature.

2.3. Sulfurization to epitaxial $BaTiO_3$ perovskite films

For the sulfurization of the $BaTiO_3$ film, we first coated a layer of thiourea solution on the surface of the as-grown film using the spin coating method (Figure 1b). The rotational speed was 2500 rpm for 30 s. After the spin-coating process, the $BaTiO_3$ film with a coated thiourea layer was thermally annealed in a box furnace at 700 °C for 15 min. The thermal treatment facilitated the diffusion of sulfur atoms from the precursor layer into the epitaxial $BaTiO_3$ film.

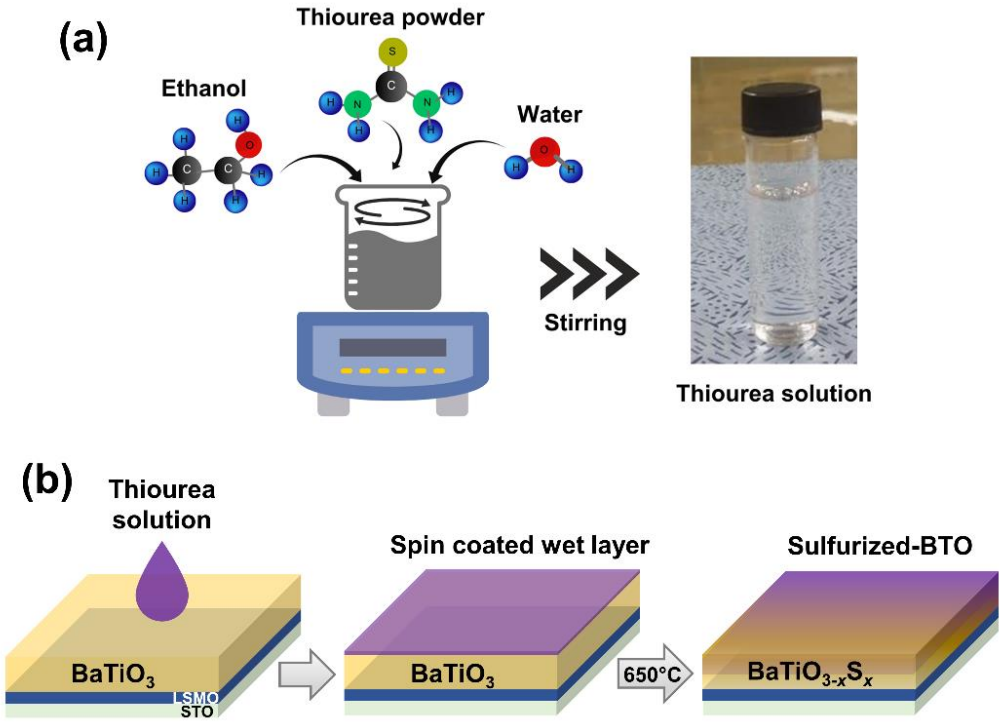

Figure 1. Sulfurization process of epitaxial perovskite $BaTiO_3$ films. (a) Preparation of the thiourea solution. (b) Fabrication of sulfurized-$BaTiO_3$ films by a spin-coating technique. The thiourea solution is coated on the film surface. Sulfur ions in the surface thiourea layer are diffused inside the $BaTiO_3$ films during thermal annealing.

2.4. Sample characterization

An X-ray diffractometer (Cu-Kα_1, D8 Discover, Bruker) was used to execute the XRD measurements of the pure and sulfurized $BaTiO_3$ films. STEM images were acquired using a STEM (JEM-ARM200F, JEOL) at 200 keV equipped with 5th-order probe corrector (ASCOR, CEOS GmbH). The probe size for atomic-scale imaging was approximately 0.8 Å. The convergence semi-angle was set at 28 mrad for STEM imaging, with the inner and outer detector angles at 10 and 20 mrad, respectively, and a camera length of 10 cm. The raw STEM images were processed by stacking 10 slices using SmartAlign and applying band-pass diffraction filtering to reduce background noise (SmartAlign and Filters Pro, HREM Research Inc., Japan). An interplanar spacing was calculated from raw STEM images by ImageJ software. The ferroelectric measurements were performed using a ferroelectric tester (PRECISON LC Material Analyzer, Radiant Technologies, USA) by applying a

triangular electric pulse with an amplitude of 15 V and a frequency of 1 kHz. An atomic force microscopy (Nanonav II station, SII NanoTechnology Inc., Japan) machine was used to characterize the surface morphology of films. X-ray photoelectron spectroscopy (XPS) was conducted using a *K*-Alpha + XPS system (Thermo Fisher Scientific, Inc., UK) equipped with a monochromated Al-Kα X-ray source ($h\nu$ = 1486.6 eV). The carbon C 1*s* peak of hydrocarbon at a binding energy of 284.6 eV was used as a reference.

3. Results and discussion

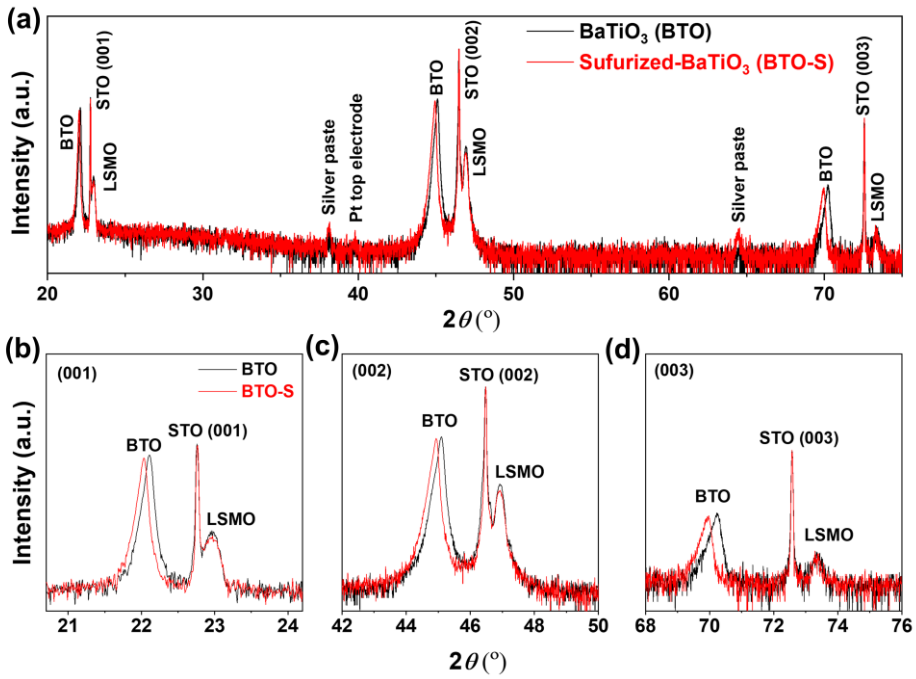

Figure 2. Structure characterization of the pure and sulfurized $BaTiO_3$ films on $LSMO/SrTiO_3$ substrates. (a) Out-of-plane θ-2θ XRD patterns of pure and sulfur-doped $BaTiO_3$ films on LSMO/STO substrates. (b–d) The enlarged (001), (002), and (003) diffraction peaks of pure and sulfurized epitaxial $BaTiO_3$ films.

Figure 2 shows the XRD θ-2θ scans of the pure and sulfur-doped $BaTiO_3$ films on LSMO/STO (001) substrates. The obtained XRD results confirm that both pure and sulfurized $BaTiO_3$ films are epitaxially grown on the substrates with *c*-axis-oriented domains. It should be noted that to examine the ferroelectric properties of $BaTiO_3$ films, we deposit platinum (Pt) electrodes on the surface of samples and the silver paste is utilized to contact the electrical probe with the LSMO bottom electrode. Accordingly, the diffraction peaks of the silver paste (~ 38.1 and 64.5°) and Pt electrodes (~ 39.8°) arise in the measured XRD patterns. It is evident that the crystal structure of $BaTiO_3$ film is modified by sulfur doping. After sulfurization, the (00*l*) Bragg peaks of $BaTiO_3$ films shift toward a lower 2θ angle, whereas the diffraction peaks of the LSMO layer are coincident. The out-of-plane lattice constants of pure and sulfur-doped $BaTiO_3$ films are 4.016 and 4.033 Å, respectively, indicative of the elongation along the *c*-axis of tetragonal unit cells induced by S doping. To confirm the crystal structures on an atomic scale, we performed annular dark field (ADF)-STEM measurements of pure

and sulfur-doped $BaTiO_3$ films. We note that the thicknesses of LSMO and $BaTiO_3$ layers are around 15 and 42 nm, respectively, as shown in Figure 3a,b. The magnified cross-sectional STEM images obviously verify the epitaxial $BaTiO_3$ films before and after a sulfurization process (Figure 3c,d). Furthermore, the in-plane lattice constants are estimated from the STEM data (Figure 3e,f). The average interplanar spacing along [100] direction (i.e., the estimated *a* lattice parameter) is approximately 3.966 and 3.970 Å for pure and sulfurized $BaTiO_3$ films, respectively. Considering that the ionic radius of sulfur ions is larger than that of oxygen ions, sulfur substitution induces a distortion in the tetragonal perovskite structures [8]. Based on our analyses of the crystal structure, the variation of in-plane (*a*) lattice constants is small compared with a significant increase in out-of-plane (*c*) lattice constants, which is quite consistent with the previous theoretical prediction in sulfur-doped perovskite oxides with a tetragonal symmetry [8]. Additionally, the calculated *c*/*a* value of epitaxial $BaTiO_3$ films increases from 1.013 to 1.016 after sulfuration. This result indicates that tetragonal lattice structures of $BaTiO_3$ films are deformed by S doping with enhanced tetragonality, which accompanies a notable increase in *c* lattice constants.

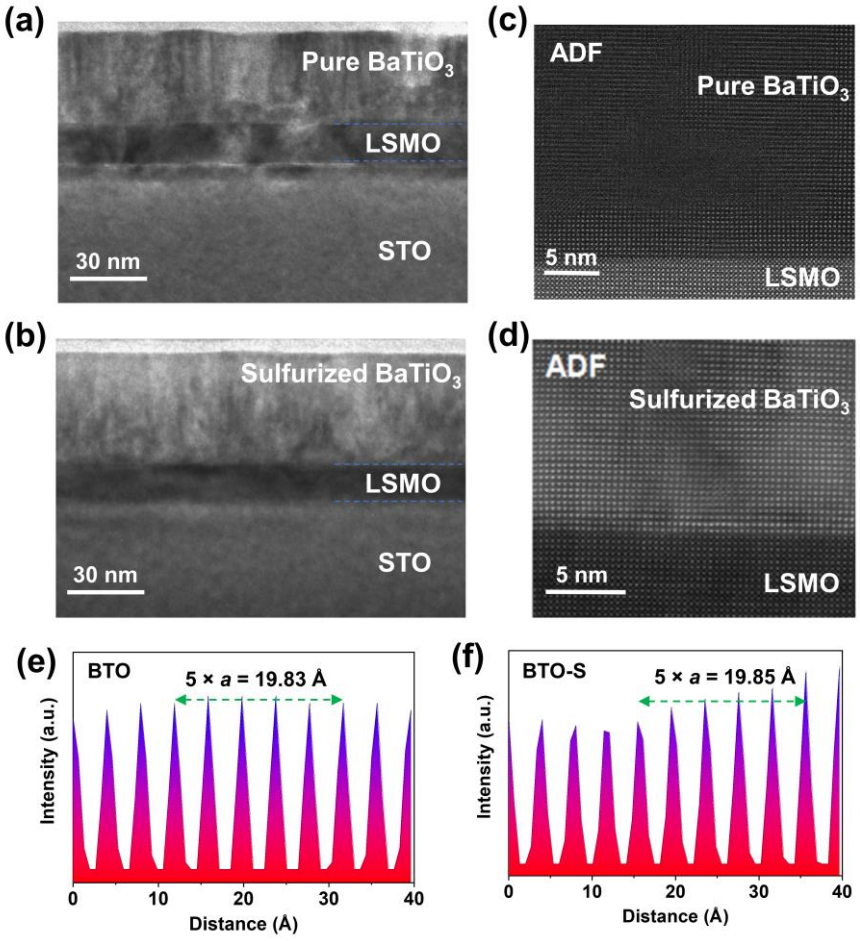

Figure 3. (a, b) Cross-sectional STEM images of the pure and sulfurized $BaTiO_3$ (~ 42 nm) films on LSMO (~ 15 nm)/$SrTiO_3$ substrates. (c, d) Magnified ADF-STEM images of pure and sulfur-doped $BaTiO_3$ films. STEM images confirm epitaxial $BaTiO_3$ films before and after a sulfurization. (e, f) Interplanar spacing along in-plane directions derived from the corresponding STEM images of (c) pure and (d) sulfur-doped $BaTiO_3$.

To confirm the presence of sulfur ions in sulfurized $BaTiO_3$ films, we carried out the XPS analyses, as shown in Figure 4. While no S signal was obtained in the XPS spectra of pure films (marked by blue solid squares), the XPS peaks of multivalent S states are observed in sulfur-doped $BaTiO_3$ films (marked by red open circles). The isovalent S state (binding energy of ~ 160.9 eV) is attributed to the sulfur dopants at oxygen sites [20,21]. We also note that the S^{4+} and S^{6+} valent states (binding energy of ~ 165.8 and 167.5 eV, respectively) would arise from sulfur species [e.g., sulfur dioxide (SO_2) and sulfur trioxide (SO_3)] adsorbed on the sample surface after a sulfurization process [21,22].

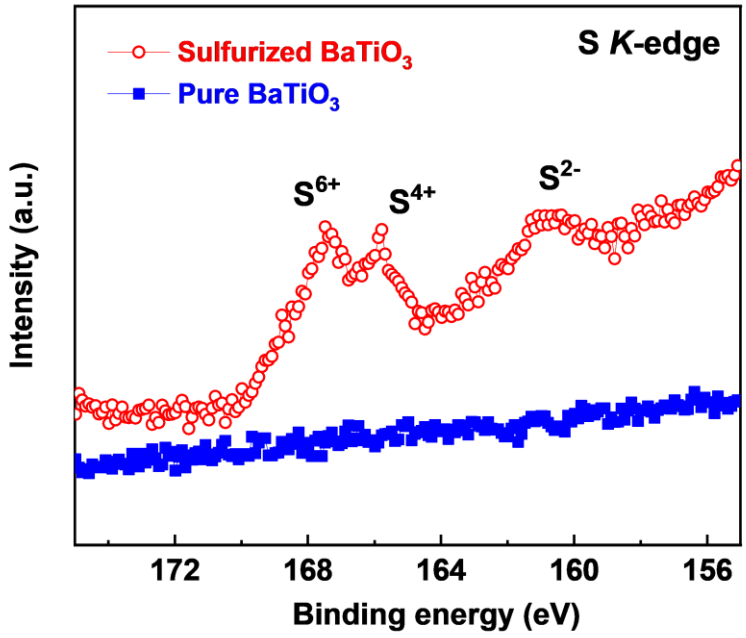

Figure 4. XPS spectra of pure and sulfur-doped $BaTiO_3$ film at a S *K*-edge. The XPS peaks corresponding to the multivalent S states are obtained in sulfurized $BaTiO_3$ films, while there is no signal of a sulfur element in pure $BaTiO_3$ films.

To check the change of surface morphology in films by the sulfurization technique, we performed AFM measurements of the epitaxial $BaTiO_3$ film before and after sulfurization, as shown in Figure 5. To ensure the quality of the epitaxial growth of $BaTiO_3$ films, the treated $SrTiO_3$ substrates with the surface-step-terrace topography were used for the film deposition (Figure 5a). Figure 5b shows the AFM topological image of the $BaTiO_3$/LSMO/STO heterostructure. It is clear that the terrace-shaped structure is still observed on the film surface with low roughness [root mean square (RMS) ~ 0.38 nm], indicative of the highly epitaxial $BaTiO_3$ film on the LSMO/STO substrate. We found that the surface morphology of epitaxial $BaTiO_3$ film is distinctly changed after sulfurization (Figure 5c). The surface of sulfur-doped $BaTiO_3$ film becomes rougher with a high RMS value of ~ 3.15 nm. The AFM data demonstrate that the surface topography of thin film is significantly affected by this sulfurization method. Considering that the sulfur ions from a thiourea-covered layer are diffused inside the $BaTiO_3$ film under thermal annealing, the diffusion process for sulfurization would be inhomogeneous in the whole film, leading to the non-uniform surface of sulfur-doped $BaTiO_3$. Furthermore, the formation of adsorbed sulfur compounds could roughen the sample surface of the sulfurized film (Figure 5c).

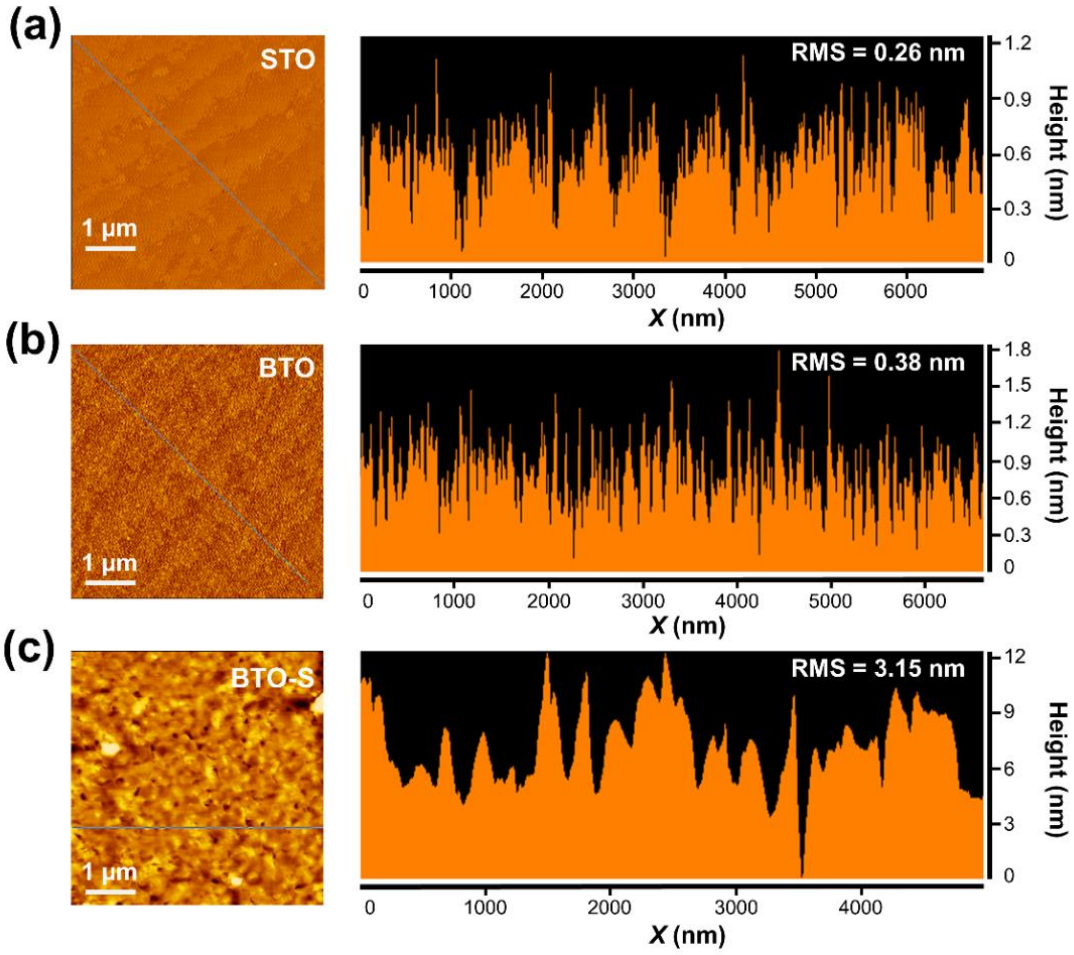

Figure 5. Surface morphology characteristics of sulfurized $BaTiO_3$ films. (a–c) AFM images of the STO substrate, the pure $BaTiO_3$ film, and the sulfurized $BaTiO_3$ film, respectively. Height profiles in the right panels are measured along the blue lines on the corresponding AFM images.

To examine how sulfurization influences the ferroelectric characteristics of epitaxial $BaTiO_3$ films, we measured polarization (P)-voltage (V) and the corresponding current (I)-voltage (V) curves in pure and sulfur-doped $BaTiO_3$ films. To perform the ferroelectric analyses, the Pt electrodes were deposited on the sample surface as top electrodes. We applied a triangle waveform with a frequency of 1 kHz and an amplitude of 15 V for P-E and I-V measurements (for details of ferroelectric measurements, see Figure 6a).

We obtained the enhancement of ferroelectric polarization in $BaTiO_3$ films by sulfurization. Both pure and sulfur-doped $BaTiO_3$ films exhibit the typical P-V hysteresis loops and I-V curves of ferroelectricity (Figures 6b,c). The sulfur-doped $BaTiO_3$ films show larger remnant [$P_r = (P_{r+} + P_{r-})/2$] and saturated [$P_s = (P_{s+} + P_{s-})/2$] polarizations than un-doped $BaTiO_3$ films. The measured values of P_r (P_s) are approximately 17.16 (27.33) and 23.15 (35.69) μC/cm^2 for pure and sulfur-doped $BaTiO_3$. The increments in the remnant (~34.8%) and saturated (~30.6%) polarizations of sulfur-doped $BaTiO_3$ films were achieved compared to pure $BaTiO_3$ films. Additionally, it is observed that the magnitude of ferroelectric switching current peaks in the sulfurized $BaTiO_3$ is much higher than that of the pure $BaTiO_3$, as shown in Figure 6c. Moreover, the sulfurized $BaTiO_3$ films exhibit an imprint ferroelectric

behavior at room temperature evident in their corresponding *P*-*V* hysteresis and *I*-*V* loops. It should be noted that the S doping concentration at a surface region would be higher than a lower region in $BaTiO_3$ films due to the diffusion of S^{2-} ions from the top precursor-covered layer under the thermal-assisted process. Consequently, an internal built-in field in $BaTiO_3$ films could be induced, accompanying the surface layer with a high concentration of negative ionic S dopants [23,24]. One ferroelectric polarization state becomes more stable than the other under the built-in field [25]. Such asymmetric polarization states result in the observed imprint behavior in the sulfur-doped $BaTiO_3$. In cooperation with structural analyses, it is plausible that the enhanced ferroelectricity in sulfurized epitaxial $BaTiO_3$ films is closely related to the pronounced tetragonal distortion induced by sulfur doping.

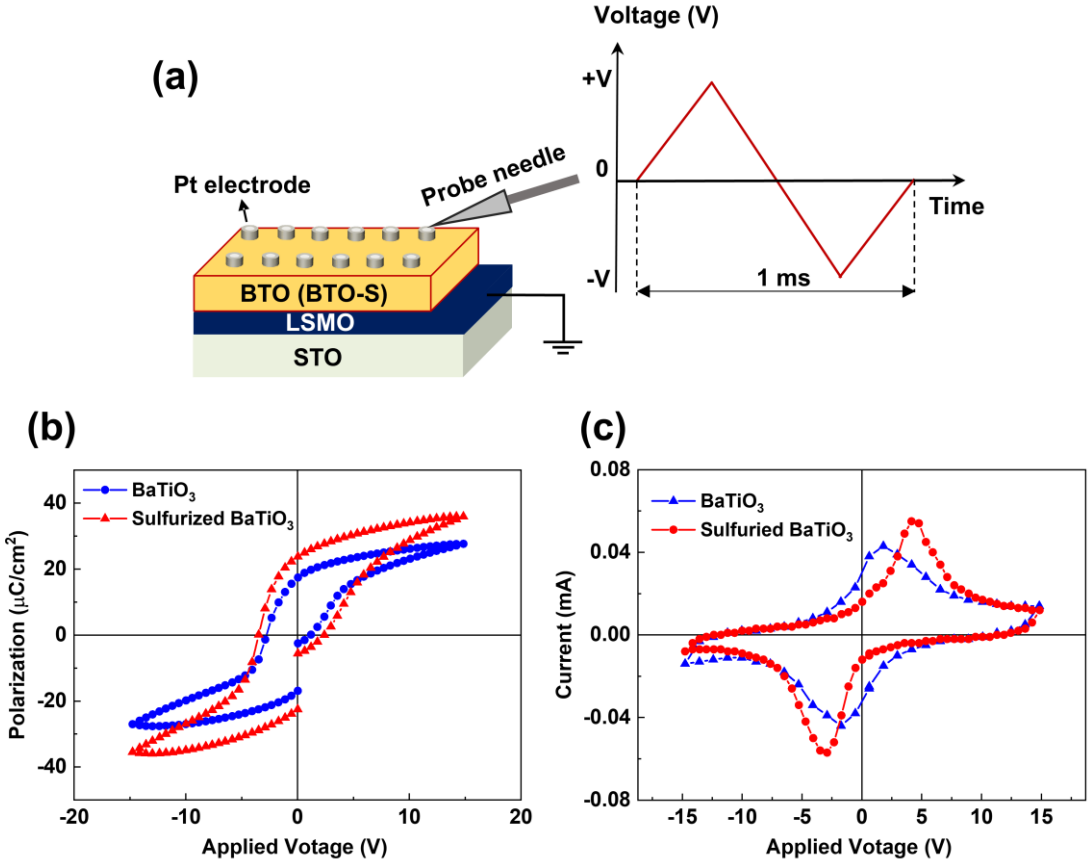

Figure 6. (a) Illustration of the experimental setup of ferroelectric measurements. Triangle pulses with an amplitude of 15 V and a frequency of 1 kHz are applied. (b) Ferroelectric hysteresis loops of pure and sulfurized $BaTiO_3$ films. (c) Corresponding current (*I*)-voltage (*V*) curves of pure and sulfur-doped $BaTiO_3$ films. The enhancement of ferroelectric polarization is observed in sulfurized $BaTiO_3$ films.

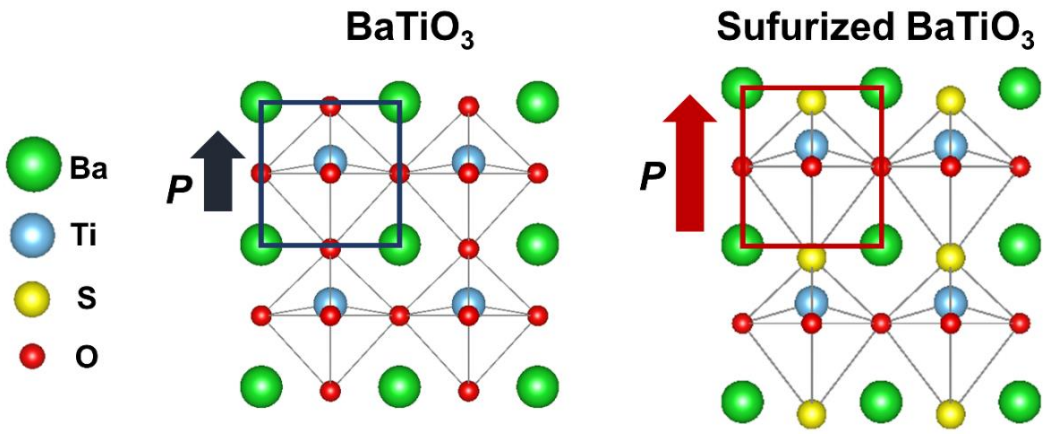

Figure 7. Schematic diagrams depicting the structural distortion in $BaTiO_3$ by the sulfur doping. The tetragonality of unit cells increases by substituting O ions with S ions accompanying an enhancement of ferroelectric polarization.

It is worthwhile to discuss a possible mechanism of enhanced ferroelectricity in epitaxial $BaTiO_3$ films by sulfurization. When the $BaTiO_3$ film is sulfurized, oxygen O atoms in the perovskite structure can be substituted by sulfur S atoms owing to the similarity in electronic configuration [8]. Moreover, previous studies reported that oxygen vacancy defects with a positive charge are highly accumulated near the top surface of ferroelectric oxide films for screening polarization charges [26]. The introduced sulfur atoms can effortlessly replace surface oxygen vacancy sites after sulfurization. We note that the ferroelectric polarization in tetragonal $BaTiO_3$ results from the off-center displacement of Ti ions due to the weakening of short-range Coulomb repulsion [27,28]. When a sulfur atom with a larger ionic radius occupies the oxygen site, the initial tetragonal unit cell of $BaTiO_3$ should be distorted and elongated along the *c*-axis (Figure 7) [8]. The structural distortion induced by sulfur doping increases tetragonality, resulting in the macroscopic change of the crystal structure in sulfurized $BaTiO_3$ film (Figure 2). Furthermore, in the substitution of a sulfur atom for an oxygen atom, the Ti ion in the tetragonal perovskite structure would become off-centered further with an increase of polar displacement and, consequently, the overall enhancement of ferroelectric polarization would be achieved in sulfur-doped $BaTiO_3$ films.

4. Conclusions

In summary, we systematically investigate the effect of sulfur doping on the ferroelectric properties of epitaxial perovskite $BaTiO_3$ thin films. The sulfurization of the high-crystalline $BaTiO_3$ films is experimentally implemented using a simple spin-coating method. The epitaxial $BaTiO_3$ films after a sulfurization process are confirmed by crystal structure analyses. The structural distortion with an increase of tetragonality is obtained in $BaTiO_3$ film induced by sulfur substitution. Intriguingly, the ferroelectricity is enhanced in sulfur-doped $BaTiO_3$ thin films accompanying the improved tetragonal distortion. Our work is of practical interest for the realization of high-efficiency ferroelectric devices.

Use of AI tools declaration

The authors declare they have not used Artificial Intelligence (AI) tools in the creation of this article.

Acknowledgments

X. L. Le, N. D. Phu and N. X. Duong acknowledge support from the VNU University of Engineering and Technology. We thank Prof. T. H. Kim and Prof. C. W. Ahn from the University of Ulsan for their support in this work.

Author contributions

All authors contributed to this work. Sample fabrication, data collection, and analysis were performed by N. X. Duong. The first draft of the manuscript was written by N. X. Duong and X. L. Le. All authors commented on previous versions of the manuscript. All authors revised and edited the final manuscript.

Conflict of interest

The authors declare no conflict of interest.

References

1. Calle-Vallejo F, Martínez JI, García-Lastra JM, et al. (2010) Trends in stability of perovskite oxides. *Angew Chem Int Ed* 49: 7699–7701. http://dx.doi.org/10.1002/anie.201002301
2. Ishihara T (2009) *Perovskite Oxide for Solid Oxide Fuel Cells*, New York: Springer New York. https://doi.org/10.1007/978-0-387-77708-5
3. Li X, Zhao H, Liang J, et al. (2021) A-site perovskite oxides: an emerging functional material for electrocatalysis and photocatalysis. *J Mater Chem A* 9: 6650–6670. https://doi.org/10.1039/D0TA09756J
4. Singh S, Singh D (2017) Structural, magnetic and electrical properties of Fe-doped perovskite manganites $La_{0.8}Ca_{0.15}Na_{0.05}Mn_{1-x}Fe_xO_3$ (x = 0, 0.05, 0.10 and 0.15). *J Alloys Compd* 702: 249–257. https://doi.org/10.1016/j.jallcom.2017.01.154
5. Wu Y, Cao G (1999) Enhanced ferroelectric properties and lowered processing temperatures of strontium bismuth niobates with vanadium doping. *Appl Phys Lett* 75: 2650–2652. https://doi.org/10.1063/1.125107
6. Rani A, Kolte J, Gopalan P (2018) Structural, electrical, magnetic and magnetoelectric properties of Co-doped $BaTiO_3$ multiferroic ceramics. *Ceram Int* 44: 16703–16711. https://doi.org/10.1016/j.ceramint.2018.06.098
7. Jana A, Sahoo S, Chowdhury S, et al. (2022) Spectroscopic comprehension of Mott-Hubbard insulator to negative charge transfer metal transition in La $Ni_xV_{1-x}O_3$ thin films. *Phys Rev B* 106: 205123. https://doi.org/10.1103/PhysRevB.106.205123

8. Brehm JA, Takenaka H, Lee CW, et al. (2014) Density functional theory study of hypothetical $PbTiO_3$-based oxysulfides. *Phys Rev B* 89: 195202. https://doi.org/10.1103/PhysRevB.89.195202
9. Shannon RD, Prewitt CT (1969) Effective ionic radii in oxides and fluorides. *Acta Crystallogr B* 25: 925–946. https://doi.org/10.1107/S0567740869003220
10. Perera S, Hui H, Zhao C, et al. (2016) Chalcogenide perovskites–an emerging class of ionic semiconductors. *Nano Energy* 22: 129–135. https://doi.org/10.1016/j.nanoen.2016.02.020
11. Li FF, Liu DR, Gao GM, et al. (2015) Improved visible-light photocatalytic activity of $NaTaO_3$ with perovskite-like structure via sulfur anion doping. *Appl Catal B-Environ* 166: 104–111. https://doi.org/10.1016/j.apcatb.2014.10.049
12. Ishikawa A, Yamada Y, Takata T, et al. (2003) Novel synthesis and photocatalytic activity of oxysulfide $Sm_2Ti_2S_2O_5$. *Chem Mater* 15: 4442–4446. https://doi.org/10.1021/cm034540h
13. Ma J, Tang K, Mao H, et al. (2018) Behavior and impact of sulfur incorporation in zinc oxysulfide alloy grown by metal organic chemical vapor deposition. *Appl Surf Sci* 435: 297–304. https://doi.org/10.1016/j.apsusc.2017.11.092
14. Wang Y, Sato N, Fujino T (2001) Synthesis of $BaZrS_3$ by short time reaction at lower temperatures. *J Alloys Compd* 327: 104–112. https://doi.org/10.1016/S0925-8388(01)01553-5
15. Itoh M, Inabe Y (2003) Optical properties and electronic structure of yttrium oxysulfide. *Phys Rev B* 68: 035107. https://doi.org/10.1103/PhysRevB.68.035107
16. Niu S, Huyan H, Liu Y, et al. (2018) Band-gap control via structural and chemical tuning of transition metal perovskite chalcogenides. *Adv Mater* 29: 1604733. https://doi.org/10.1002/adma.201604733
17. Lee SM, Cho YS (2016) Optical and grain boundary potential characteristics of sulfurized $BiFeO_3$ thin films for photovoltaic applications. *Dalton Trans* 45: 5598–5603. https://doi.org/10.1039/C5DT04585A
18. Bilgin I, Liu F, Vargas A, et al. (2015) Chemical vapor deposition synthesized atomically thin molybdenum disulfide with optoelectronic-grade crystalline quality. *ACS Nano* 9: 8822–8832. https://doi.org/10.1021/acsnano.5b02019
19. Lelieveld R, Ijdo DJW (1980) Sulphides with the $GdFeO_3$ structure. *Acta Crystallogr B* 36: 2223–2226. https://doi.org/10.1107/S056774088000845X
20. Tang X, Li D (2008) Sulfur-doped highly ordered TiO_2 nanotubular arrays with visible light response. *J Phys Chem C* 112: 5405–5409. https://doi.org/10.1021/jp710468a
21. Gonbeau D, Guimon C, Pfister-Guillouzo G, et al. (1991) XPS study of thin films of titanium oxysulfides. *Surf Sci* 254: 81–89. https://doi.org/10.1016/0039-6028(91)90640-E
22. Sayago DI, Serrano P, Böhme O, et al. (2001) Adsorption and desorption of SO_2 on the TiO_2 (110)-(1×1) surface: A photoemission study. *Phys Rev B* 64: 205402. https://doi.org/10.1103/PhysRevB.64.205402
23. Liu Y, Lou X, Bibes M, et al. (2013) Effect of a built-in electric field in asymmetric ferroelectric tunnel junctions. *Phys Rev B* 88: 024106. https://doi.org/10.1103/PhysRevB.88.024106
24. Tagantsev AK, Gerra G (2006) Interface-induced phenomena in polarization response of ferroelectric thin films. *J Appl Phys* 100: 051607. https://doi.org/10.1063/1.2337009
25. Jesse S, Rodriguez BJ, Choudhury S, et al. (2008) Direct imaging of the spatial and energy distribution of nucleation centres in ferroelectric materials. *Nat Mater* 7: 209–215. https://doi.org/10.1038/nmat2114

26. Chisholm MF, Luo W, Oxley MP, et al. (2010) Atomic-scale compensation phenomena at polar interfaces. *Phys Rev Lett* 105: 197602. https://doi.org/10.1103/PhysRevLett.105.197602
27. Cohen RE (1992) Origin of ferroelectricity in perovskite oxides. *Nature* 358: 136–138. https://doi.org/10.1038/358136a0
28. Megaw HD (1952) Origin of ferroelectricity in barium titanate and other perovskite-type crystals. *Acta Crystallogr A* 5: 739–749. https://doi.org/10.1107/S0365110X52002069

AIMS Press